Measuring Wheel/Rail Contact Stresses using Ultrasound

M.B. Marshall[1]*, R.Lewis[1], R.S. Dwyer-Joyce[1], O. Olofsson[2], S. Björklund[2]

[1]Department of Mechanical Engineering, The University of Sheffield, Mappin Street, Sheffield, S1 3JD, UK.
[2] Department of Machine Design, KTH, SE 100 44 Stockholm, Sweden.
*Corresponding author

Summary: The investigation of contact area and pressure distribution in a wheel/rail contact is essential information required in fatigue and wear calculations to determine design life, regrinding requirements, and maintenance schedules. The aim of this work was to use ultrasound to non-destructively determine wheel/rail contact pressures. Three different contacts were investigated those resulting from; un-used, sand damaged, and worn wheel/rail specimens.
A wheel/rail interface behaves like a spring. If the pressure is high the interface is very stiff, with few air gaps, and allows the transmission of an ultrasonic sound wave. If the pressure is low, interfacial stiffness is low and almost all the ultrasound is reflected.
A *spring model* was used to determine maps of contact stiffness from wheel/rail ultrasonic reflection data. Pressure was then determined using a calibration experiment. Separate calibrations were performed for each of the three sets of wheel/rail specimens investigated. Measured contact pressure distributions are compared to those determined using analytical and computer bases numerical techniques.

Index Terms: wheel/rail contact, contact pressure, ultrasound

1. INTRODUCTION

The assessment of structural integrity is a key part of mechanical engineering design. The wheel/rail contact is no exception, where an understanding of interface pressures is essential, as this information is required in both fatigue and wear calculations for the wheels and rails. These calculations in turn determine design life, re-grinding, and maintenance schedules.
Present work in this area is focused on applying analytical and computer based numerical techniques to investigate the wheel/rail contact. Experimental work, as performed in this study, is therefore beneficial as it provides a means for validating such models.

Paper from 14th International Wheelset Congress, 17-21 October, Orlando, USA.

This study aims to quantify the size and stress distribution of the wheel/rail contact by means of an ultrasonic reflection based method. Dwyer-Joyce et al. [1] performed early ultrasound work, and demonstrated the relation between contact pressure and ultrasonic reflection from a rough surface contact. Pau et al. [2] have previously applied the technique to a wheel/rail contact with some success. The work is advanced here by considering higher loadings of the contact, and by investigating un-used, sand damaged, and worn wheel/rail surface conditions. A calibration routine is employed specific to the contact surfaces, with numerical modelling of the wheel/rail contact also used as a means of validating the experimental results.

2. ULTRASONIC REFLECTION FROM AN INCOMPLETE INTERFACE

When two real engineering surfaces are loaded together, an incomplete interface occurs. The surfaces contact at asperity tips, leaving pockets of trapped air also present at the interface. When an ultrasonic wave strikes such a boundary it is partially reflected; it passes through the regions of asperity contact and is reflected back from the air gaps (Figure 1). Tattersall [3] defines the reflection coefficient, *R*, as the fraction of the incident ultrasonic signal reflected from the interface.

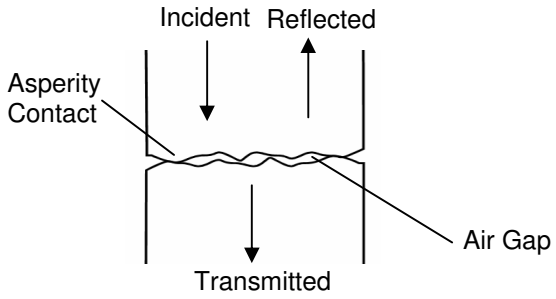

Figure 1. Ultrasonic Reflection at a Rough Surface Interface

Ultrasonic reflection from a rough surface contact is dependent on the wavelength of the incident sound signal. Kendall and Tabor [4] investigated the case where the wavelength of the ultrasound is long compared to the magnitude of the air gaps. They found for this case that the interface as a whole behaved as a reflector, and that the reflection was governed by the *spring* like behaviour of the contact. For two similar materials contacting the relation reduces to:

$$|R| = \frac{1}{\sqrt{1+(2K/\omega z)}} \qquad (1)$$

where K is the interfacial stiffness, ω the angular frequency (= $2\pi f$) of the ultrasonic wave, and z the acoustic impedance (the product of wave speed and density for the material).

Interfacial stiffness, K (expressed per unit area) is the load required to cause unit approach of the mean lines of roughness for two surfaces [5]. The stiffness of a dry interface may vary from zero to infinity. Under a light loading only a few asperity

contacts are made, it is easy to deform these asperities and decrease surface separation, thus stiffness is low. As the surface load increases, more asperities contact and it becomes harder to reduce surface separation, and the stiffness has now increased. Finally when the surfaces are pressed together to such an extent that the interface is complete, the stiffness becomes infinite, as the separation can no longer be reduced. Therefore, for a given pair of contacting surfaces, the stiffness depends on the load applied to them, and hence the contact pressure between them. However, the stiffness also depends on the size, number, and distribution of the asperities within the contact. There is thus no single relation between interfacial stiffness and contact pressure.

Drinkwater et al. [6] investigated the *spring* model and its applicability to ultrasonic reflection data from a rough surface interface. They demonstrated that it could be applied to reflection data up to frequencies of 50MHz. Further, they showed a calibration experiment could be performed to find the relation between interfacial stiffness and pressure for a given pair of rough contacting surfaces. The work of Hodgson et al. [7] also showed that, for the first loading of a pair of surfaces below bulk yield stress, the contact pressure and stiffness are proportional.

3. EXPERIMENTAL DETAILS

3.1 Ultrasonic Scanning Apparatus

The ultrasonic equipment used to investigate the wheel/rail contact consisted of an ultrasonic transducer, an oscilloscope, an ultrasonic pulser-receiver (UPR), and a PC to which ultrasonic signals were downloaded. A 10MHz spherical focusing transducer was used as the ultrasonic source. The ultrasound was generated within the transducer by a piezo-electric crystal, that produced the sound wave in response to a voltage excitation. Reflected ultrasonic signals are also received back from the interface by the same transducer. When focused on the wheel/rail contact the ultrasonic spot diameter was 0.9 mm, this was the resolution of the technique.

The transducer was mounted on an *xy* scanning system. Stepper motors linked to the PC controlled the position of the transducer along these two axes. In this way, ultrasonic measurements were made at a series of discrete points within a prescribed area. The vertical height of the transducer was set manually. Figure 2 shows a schematic illustration of the equipment.

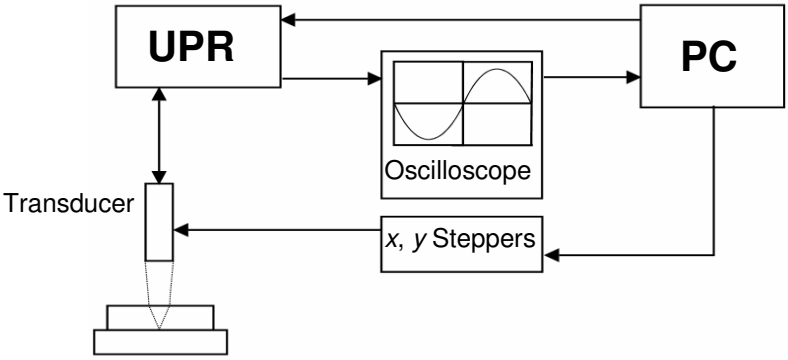

Figure 2. Schematic of Ultrasonic Scanning Apparatus

3.2 Contact Scanning

Sample wheel and rail specimens were cut from actual wheels and rails. In this work three different wheel/rail contacts were investigated; those resulting from un-used, sand damaged, and worn specimens. Figure 3 shows the loaded interface between a pair of specimens being scanned. As shown the transducer is mounted in a water bath above the specimens, and is so positioned to focus the ultrasonic signal onto the interface between them. The water also acts as a couplant, and is required due to the rapid attenuation of ultrasound in air. In this series of experiments the contacts were hydraulically loaded normally in the range 20-80kN, this is typical of what they would experience in operation.

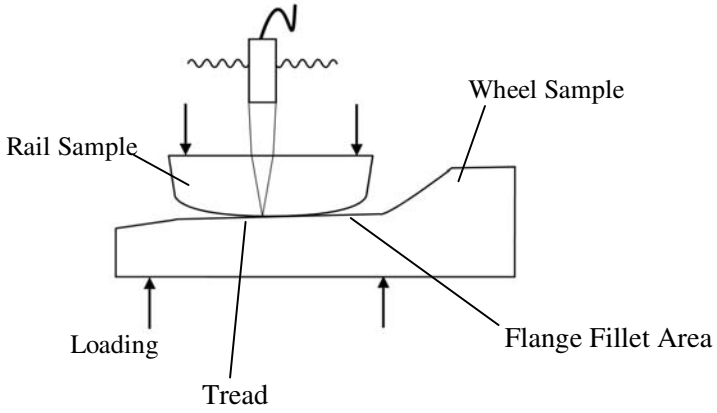

Figure 3. Scanning of the Wheel/Rail Contact

The transducer was scanned over the contact area, with the amplitude of the reflected sound wave recorded at 0.25mm intervals. The amplitude of the reflected pulse received back at the transducer is lower than the emitted value. This is because the sound wave is partially transmitted at the wheel/rail interface, as well as being attenuated as it travels in the material bulk. A reference trace was also recorded on the interface from a point to the side of the wheel and rail contact region. The reference trace is only diminished by attenuation, as all the ultrasound is reflected from the steel-air interface at this point. If the reflected trace from the contact is divided by the

reference value, the attenuation is cancelled. This leaves the fraction of ultrasound incident at the interface that is reflected from it, that is the reflection coefficient, *R*. In this way, reflection coefficient maps of the interface were constructed at each loading from the reflected voltage data.
Applying Equation 1 to the reflected voltage data from the contact produced interfacial stiffness maps.

3.3 Calibration

A calibration experiment, as described in Marshall et al. [8], was performed to find the relationship between interfacial stiffness and contact pressure for the wheel/rail specimens. The calibration specimens were machined from the same material and to the same surface finish as the wheel/rail components. Due to the differing surface finishes of the un-used, sand damaged, and worn specimens a separate calibration experiments were performed for each case. When the worn specimens were loaded together a twin contact patch was observed, consisting of both tread and flange fillet components. Separate calibrations were performed for these two contacts, since the wear and resulting surface finish was different at these points.
Figure 4 shows the calibration curve for the sand damaged specimens. As shown over this pressure range the stiffness-pressure relationship is approximately linear. The empirical equation for the line of best fit through the experimental data is $p = 263K$. It relates the contact pressure, p, to interfacial stiffness, K. Similar linear relations were found for the other wheel/rail interfaces. These were $p = 418K$, $p = 123K$, and $p = 198K$, for the un-used, worn tread, and worn flange fillet contacts respectively. These calibration relationships were used to produce contact pressure maps from the wheel/rail scans.

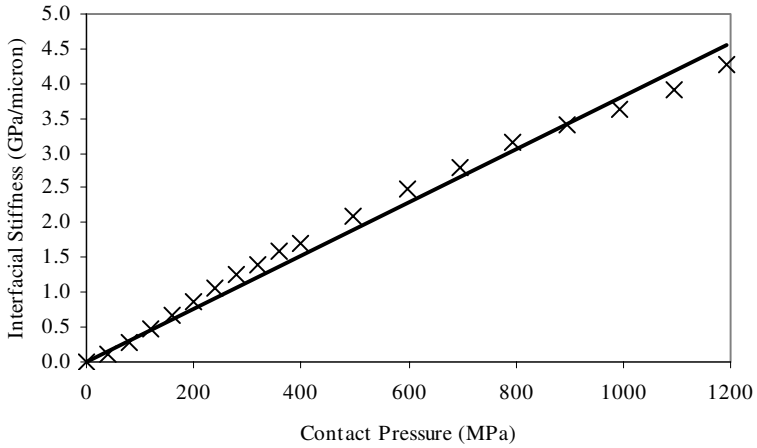

Figure 4. Sand Damaged Interfacial Stiffness-Contact Pressure Calibration

4. CONTACT MODELLING

A 3D stylus instrument is used to measure the surface topography of an area that is larger than the anticipated contact area of the contacting bodies. The digitised topography is used as the input to a contact computation program [9] that works by replacing the continuous pressure distribution with a discrete set of elements. The contact computation applies to normally loaded, frictionless contacts, by modelling the interacting bodies as infinite half-spaces. This assumption requires that the region of contact is small compared to the size of the bodies. It is well known that asperity contacts are accompanied by high local pressures, resulting in plastic deformation, even for small contact interaction forces. Thus, the contact program was modified to take plastic deformations into account. The anticipated contact area is divided into N rectangular cells, each of these being subjected to a uniform unknown pressure. Knowing the gap vector $\boldsymbol{h}$ between the cells before deformation and the applied normal displacement, δ_z, the solution is obtained from an equation system which written in matrix form becomes:

$$\boldsymbol{Cp} = \delta_z - \boldsymbol{h} \equiv \boldsymbol{d} \qquad (2)$$

where $\boldsymbol{C}$ is the influence matrix and $\boldsymbol{p}$ a vector with the unknown pressures. The influence coefficient C_{ij} relates the deformation at cell i due to a unit pressure in cell j. The sizes and shapes of the real contact areas are not known in advance. An initial estimate, which will contain the true contact region, is the contact area obtained if the bodies are allowed to penetrate each other without any interaction. When solving Equation 2, the pressures at cells outside the true contact region become negative. These cells are removed and the equation system is solved iteratively until all pressures are positive.

In contacts between rough surfaces it is often found that the pressure in some cells is excessively large, implying that the deformation is plastic rather than elastic. An approximate method to account for this is to limit the allowable pressure by a yield pressure P_y. Thus, Equation 2 is first solved according to the procedure outlined above, removing all cells having negative pressures. The resulting pressures are inspected and all pressures exceeding the yield pressure P_y are removed from the equation system. However, the cells with plastic behaviour do still contribute to the deformation at the elastic cells and Equation 2 thus becomes:

$$\boldsymbol{C_{ee}p_e} = \boldsymbol{d_e} - \boldsymbol{C_{ep}p_p} \qquad (3)$$

where the subscripts e and p contains indices to cells with elastic and plastic behaviour respectively. For example $\boldsymbol{C_{ep}}$ denotes the rows of $\boldsymbol{C}$ that correspond to cells with elastic deformation and the columns that correspond to plastic deformation. Equation 3 is repeatedly solved until all pressures are positive and less or equal to P_y.

Other researchers [10 - 13] have described similar or more elaborate methods to account for plasticity in contact pressure calculations. The method described above is very simple, and can only be considered as an approximate representation of the true plastic behaviour in rough contacts. It is however believed that when the plastic deformations are small and limited to a minor part of the contact area, the approximate method described above is sufficiently accurate for the purpose of this work.

5. RESULTS

5.1 Ultrasonic Results

Figure 5 shows the contact pressure maps from the un-used wheel/rail specimens at loadings of 40, 60, and 80kN. Also marked on the Figure is the predicted Hertzian elastic contact patch for the two bodies (for calculation see Johnson [14]).

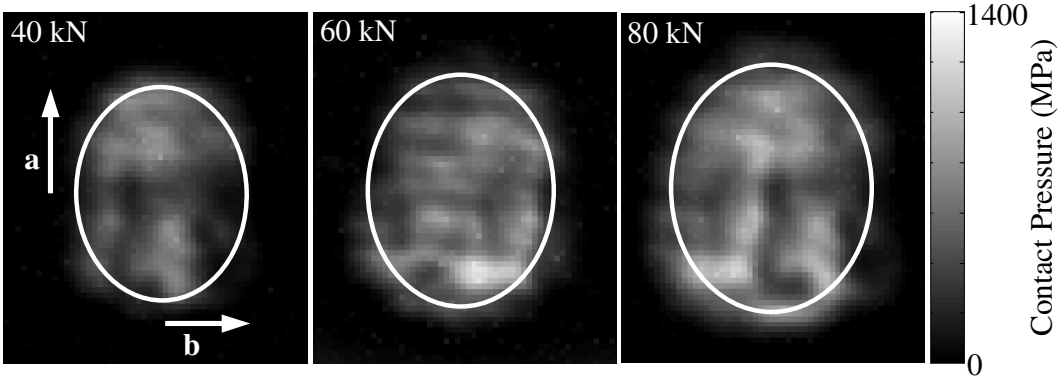

Figure 5. Un-Used Wheel/Rail Contact Pressure Maps

As shown there is good geometric agreement between the analytically predicted and measured contact patches. However, when comparing to Hertz, the measured contact is to a small degree fragmented. This is due to an initial surface roughness present on the un-used rail specimen. The roughness produces a less conformal contact, leading to higher measured maximum contact pressures than those predicted by theory (see Table 1).

Load (kN)	Hertzian Contact Geometry		Hertz p_{max} (MPa)	Measured p_{max} (MPa)
	a (mm)	b (mm)		
40	4.5	3.7	787	950
60	5.2	4.2	901	1329
80	5.7	4.6	992	1242

Table 1. Measure and Predicted Maximum Pressures

A check can also be made on the validity of the calibration procedure. The pressure distribution of the contact has been ultrasonically measured at each loading. Therefore, by integrating the pressure distribution the total load supported by the interface can be determined. Once the measured load has been calculated it can be compared to the hydraulic load the test was performed at. The correlation was found to be good at all interface loadings as shown in Figure 6, where the comparisons for new and sand damaged specimens are shown.

Figure 7 shows contact patches measured at a load of 65kN from the un-used, sand damaged, and worn wheel/rail specimens. Key data from the contacts is shown in Table 2, a Hertzian contact analysis has not been performed for the sand damaged and worn cases due to the non-constant radii of curvature of the specimens.

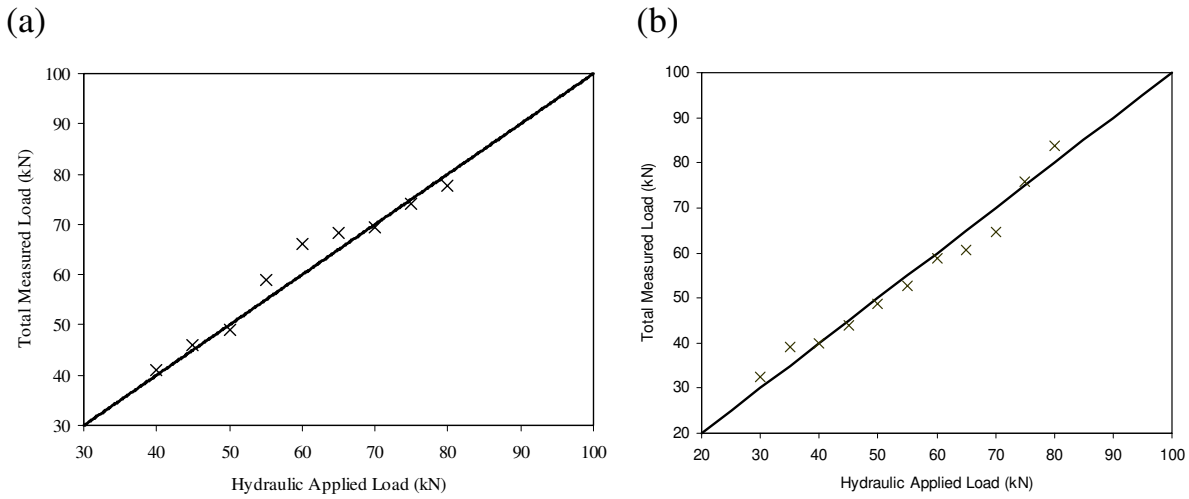

Figure 6. Applied and Measured Load Comparison (a) New Specimens and (b) Sand Damaged Specimens

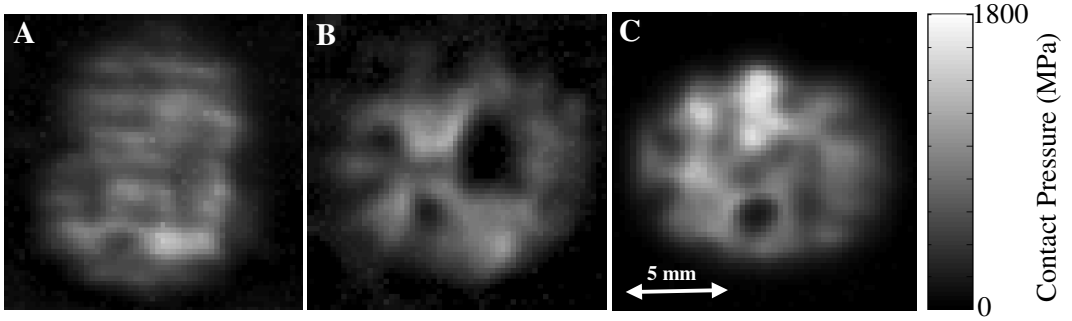

Figure 7. Wheel/Rail Contact at 65 kN for a) Un-Used; b) Sand Damaged; c) Worn Specimens.

When comparing the contact patch from the un-used specimens to that from the sand damaged interface there are marked differences. Although the load supported is similar, the contact patch is extremely fragmented. The sand damage leads to an extremely rough surface and a generally patchy contact. There are now large areas within the contact patch where the wheel and rail are no longer touching, leading to a spread in the contact. Due to a slightly increased real area of contact, the peak pressure is also reduced.

The worn wheel/rail specimens give a different result when compared to the un-used case. Both the wheel and rail wear in use, leaving a smooth polished surface on both specimens. However, because of the many different relative positions between the wheel and rail in the train's operation, the wear has a random nature and does not lead to a more conformal contact. Instead waviness is introduced in the wheel surface, and its effect is shown in the worn contact patch shown in Figure 6c. On a global scale the wear causes the relative radii of the two surfaces to increase, giving a more circular contact patch with a larger real area of contact. However, locally the surface waviness leads to fragmentation, and it is this that leads to a higher peak pressure than seen for the un-used contact patch. The waviness causes an imbalance in the contact patch load distribution.

	Wheel/Rail Contact	Measured Load (kN)	Area (mm^2)	p_{max} (MPa)
Single Contacts	Un-Used	64	138	1423
	Sand Damaged	65	164	1228
	Worn	64	207	1669
Double Contact	Worn-Tread	46	166	1144
	Worn-Flange Fillet	17	71	1114
	Worn Total	63	237	1144

Table 2. Wheel/Rail Contact Loading and Geometry

Figure 7a shows the single contact from the worn specimens, with Figure 7b showing the twin contact also recorded. The twin contact patch occurred when the rail specimen was moved toward the flange fillet area of the wheel component. When comparing Figures 7a and b, the introduction of the second contact causes the load supported and the real area contact at the tread to reduce. As shown in Table 2, approximately 30% of the total load is now supported in the second contact, with a similar fraction of the total real area of contact occurring there. This reduces the intensity of the peak pressures in the tread contact. The overall real area of contact is also increased slightly for the twin contact when compared to the single case. All this is in good qualitative agreement with simulation results of two point contacts presented by Telliskivi & Olofsson [15]. Due to the concave radius of curvature of the wheel specimen near the flange, the second contact resembles a line. As shown in Figure 7b and Table 2 the peak pressure is similar in each component of the double contact.

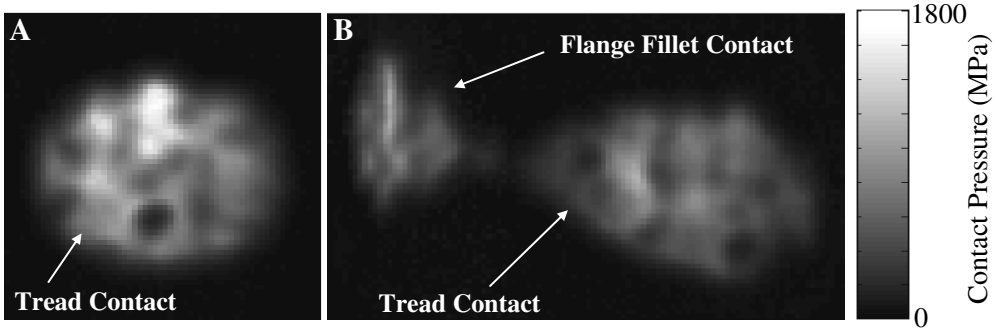

Figure 7. Worn Wheel/Rail Contact at 65 kN (a) Single Contact and (b) Double Contact.

5.2 Contact Model Comparison

Boundary element modelling was performed for the un-used wheel/rail specimens. Figure 8 compares the ultrasonic results to those from the modelling at a load of 80kN, also included on the Figure is the predicted Hertz solution.

As shown there is good global geometric correlation, all the contact patches have similar real areas of contact. The numerical modelling also predicts a fragmented contact patch as determined using the ultrasound. This is because the computational package includes the effects of the surface roughness and damage, as it is based on

the real surface topography. The fragmentation is not present in the Hertzian contact patch as it assumes perfectly smooth contacting surfaces. Although the degree of fragmentation is similar between the model and experiment, local correlation is poor. This is likely due to slightly different relative surface positions in the model and experiment.

Contact pressures can also be compared between the ultrasonic results and numerical model. Included on Figure 8 are both the elastic and elastic-plastic model cases. The elastic case assumes no localised yielding in the contact; this results in peak contact pressures well in excess of the yield value for the material. This is physically unlikely and contradicts the ultrasonic measurements. However, the elastic-plastic case shows similar peak pressures to the experiment. The model and experimental peak pressures are in excess of those predicted by the Hertzian solution, this is due to the reduced interface conformity attributable to surface roughening.

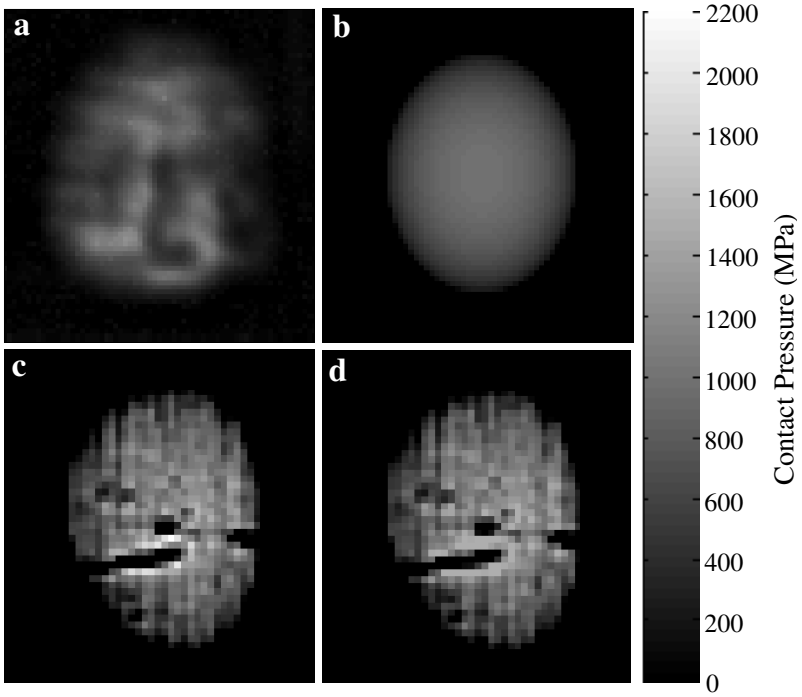

Figure 8. Contact Pressure Maps for a load of: 80 kN (a) Ultrasonic Measurement; (b) Hertzian; (c) Elastic Model; (d) Elastic-Plastic Model.

6. DISCUSSION

The work described has shown a means to non-intrusively determine the wheel/rail contact pressure distribution. When compared with established analytical theory and numerical techniques the ultrasonic results correlate well. As part of this work the effect, with regard to the contact patch, of wear and sand damage on the wheel/rail interface was investigated. The study showed that these two factors had a pronounced effect on the contact patch, often leading to its fragmentation. This in turn leads to increased peak pressures at the interface, as it is less conformal. These higher pressures may

lead to accelerated fatigue and wear damage, highlighting the benefit of re-grinding programs for both wheels and rails.
Here the contact has been modelled statically and scanned using a single transducer. The technique is limited by the resolution of the ultrasonic probe. However, the contact between the wheel and the rail is large with gradual pressure changes, hence the effects of the spot size are negligible. The application of this technique to a moving contact would be difficult. Although an array of transducers could be used to remove the need for scanning, mounting the transducers and focusing the ultrasound could be problematic. However, a wide beam transducer could be used to investigate specific areas of the wheel/rail interface, for example, the time the wheel flange spends in contact with the railhead. This type of information could help to build a picture of the variety of loadings the wheel experiences and where they occur.

7. CONCLUSIONS

- A method has been established to determine interface pressures in a wheel/rail contact. The method uses the measurement of a reflected ultrasonic signal and a parallel calibration procedure.

- The experimental results for the un-used wheel/rail specimens show good agreement with a numerical model when comparing both overall contact size and peak pressures.

- Surface roughness effects influence the wheel/rail contact pressure distribution. Wear and sand damage fragment the contact, leading to a less conformal interface and higher peak pressures.

8. REFERENCES

[1] Dwyer-Joyce, R.S., Drinkwater, B.W. "Analysis of Contact Pressure using Ultrasonic Reflection", Experimental Mechanics, *Proceedings of 11th Annual Conference on Experimental Mechanics*, 1998, Balkema, Rotterdam, pp747-754.

[2] Pau, M., Aymerich, F., Ginesu, F., "Ultrasonic Measurement of Nominal Contact Area and Contact Pressure in a Wheel/Rail System", *Journal of Rail and Rapid Transit, Proceedings of the IMechE*, 2000, Vol. 214, pp 231-243.

[3] Tattersall, A.G. "The Ultrasonic Pulse-Echo Technique as Applied to Adhesion Testing", *J. Phys. D: Appl. Phys*, 1973, Vol. 6, pp819-832.

[4] Kendall, K. and Tabor, D. "An Ultrasonic Study of the Area of Contact between Stationary and Sliding Surfaces", *Proceedings of the Royal Society*, Series A, 1971, Vol. 323, pp321-340.

[5] Thomas, T.R., Sayles, R.S. "Stiffness of Machine Tool Joints: A Random-Process Approach", Trans. *ASME, J. Eng. Ind.*, 1977, Paper No. 76-WA/Prod-23.

[6] Drinkwater, B.W., Dwyer-Joyce, R.S., Cawley, P. "A Study of the Interaction between Ultrasound and a Partially Contacting Solid-Solid Interface",

Proceedings of the Royal Society Series A, 1996, Vol. 452, No. 1955, pp. 2613-2628.

[7] Hodgson, K., Dywer-Joyce, R.S., Drinkwater, B.W., "Ultrasound as an Experimental Tool for investigating Engineering Contacts", *Proceedings of the 9th Nordic Symposium on Tribology, 'Nordic 2000'*, Eds. Andersson, P., Ronkainen, H., Holmberg, K., 2000, Vol. 2, pp377-386.

[8] Marshall, M. B., Lewis, R., Dwyer-Joyce, R. S., Olofsson, U., Björklund, S., "Ultrasonic Characterisation of a Wheel/Rail Contact", *Proceedings of the 30th Leeds-Lyon Symposium on Tribology*, 2003.

[9] Björklund, S., Andersson, S., "A Numerical Method for Real Elastic Contacts Subjected to Normal and Tangential Loading", *Wear*, 1994, Vol. 179, pp. 117-122

[10] Lee, S.C., Ren, N., "Behaviour of Elastic-Plastic Rough Surface Contacts as Affected by Surface Topography, Load and Material Hardness", *Tribology Transactions*, 1996, Vol. 39, No. 1, pp. 67-74.

[11] Poon, C.Y., Sayles, R.S., "Numerical Contact Model of a Smooth Ball on an Anisotropic Surface", *Journal of Tribology*, 1994, Vol. 116, pp. 194-201.

[12] Yu, M.M.H., Bushan, B., "Contact Analysis of Three-dimensional Rough Surfaces Under Frictionless and Frictional Contact", *Wear*, 1996, Vol. 200, pp. 265-280.

[13] Bucher, F., "The Contact Between Micro-Rough Rails and Wheels", Doctoral thesis, Mechanical Engineering and Transport Systems, Berlin Technical University, 2002.

[14] Johnson, K.L., *Contact Mechanics,* Cambridge University Press, 1985.

[15] Telliskivi T, Olofsson U., "Contact Mechanics Analysis of Measured Wheel-Rail Profiles using the Finite Element Method", *Proceedings of the IMechE Part F, Journal of Rail and Rapid Transit*, 2001, Vol. 215, pp. 65-72.